Prefusion conformation of SARS-CoV-2 receptor-binding domain favours interactions with human receptor ACE2

Nitesh Kumawat[1], Andrejs Tucs[2], Soumen Bera[3], Gennady N. Chuev[6], Marina V. Fedotova[7], Koji Tsuda[2], Sergey E. Kruchinin[7], Adnan Sljoka[4,5*], Amit Chakraborty[8*]**

[1]School of Mathematics, Statistics and Computational Sciences, Central University of Rajasthan, Bandarsindri, Ajmer, India.

[2]Graduate School of Frontier Sciences, The University of Tokyo, Kashiwa, Chiba, Japan

[3]Department of Microbiology, University of Tennessee, Knoxville, USA

[4]RIKEN Center for Advanced Intelligence Project, Tokyo, Japan.

[5]Department of Chemistry, University of Toronto, Toronto, Canada.

[6]Institute of Theoretical and Experimental Biophysics, Russian Academy of Sciences, Pushchino, Russia.

[7]G.A. Krestov Institute of Solution Chemistry, Russian Academy of Sciences, Ivanovo, Russia.

[8]Department of Mathematics, School of Physical Sciences, Sikkim University, Gangtok, India

***Corresponding author:**
***Amit Chakraborty**
E-mail: achakraborty@cus.ac.in; amitc.envsc@yahoo.com

***Adnan Sljoka**
E-mail: adnan.sljoka@riken.jp

**Co-corresponding author:
Gennady N. Chuev
E-mail: genchuev@rambler.ru

Lead contact:
Amit Chakraborty
E-mail: achakraborty@cus.ac.in

ABSTRACT

A new coronavirus epidemic COVID-19 caused by Severe Acute Respiratory Syndrome coronavirus (SARS-CoV-2) poses serious threat across continents, leading to the World Health Organization declaration of a Public Health Emergence of International Concern. In order to stop the entry of the virus into human host cell, major therapeutic and vaccine design efforts are now targeting interactions between the SARS-CoV-2 spike (S) glycoprotein and the human cellular membrane receptor angiotensin-converting enzyme, hACE2. By analysing cryo-EM structures of SARS-CoV-2 and SARS-CoV-1, we report here that the homotrimer SARS-CoV-2 S receptor-binding domain (RBD) that bind with hACE2 has expanded in size with a large conformational change of its AA residues relative to SARS-CoV-1 S protein. Protomer with the up-conformational form RBD that only can bind with hACE2 showed higher intermolecular interactions at the interface, with differential distributions and the inclusion of two specific H-bonds in the CoV-2 complex. However, these interactions are resulted in significant reductions in structural rigidity, favouring proteolytic processing of S protein for the fusion of the viral and cellular membrane. Further conformational dynamics analysis of the RBD motions of SARS-CoV-2 and SARS-CoV-1 point to the role in modification in the RBD conformational dynamics and their likely impact on infectivity.

Keywords: SARS; Coronavirus; Structural rigidity; Normal mode analysis; Conformational Dynamics.

Introduction

Severe Acute Respiratory Syndrome coronavirus (SARS-CoV-2) is associated with the current disease outbreak COVID-19 that spread over more than 200 countries and infected several millions of people worldwide. The first coronavirus outbreak of SARS-CoV-1occurred in 2002 and the second outbreak of Middle East Respiratory Syndrome coronavirus (MERS-CoV) was in 2012. Rapid human-to-human transmission of SARS-CoV-2 across the continents has leaded the World Health Organization (WHO) declaration of Public Health Emergence of International Concern on January 30th, 2020. Although there is large heterogeneity in disease transmission, SARS-CoV-2 spread is much faster relative to the other two previous outbreaks [1,2]. Here we identify essential structural differences that contribute to higher transmissibility of SARS-CoV-2 relative to SARS-CoV-1.

Coronavirus (CoV) entry into human host cell is mediated by the transmembrane spike (S) glycoprotein protruding from the viral surface. With the use of this S protein, which is a trimeric class I fusion protein, CoV-1hijack the human receptor membrane protein angiotensin-converting enzyme 2(hACE2) highly expressed in lungs, heart, kidneys and intestine cells [3]. The S protein protomer is made of two subunits, S1 and S2, which are responsible for receptor recognition and membrane fusion. The S1 unit comprises the receptor-binding domain (RBD) that bound with the peptidase domain (PD) of hACE2 and it contributes to stabilization of the prefusion conformation state. Receptor-binding destabilizes the prefusion state, resulting in shedding of S1 unit and priming of S2 for membrane fusion. S-protein is then cleaved further by the host proteases at S2' site located immediately upstream of the fusion peptide, triggering the protein for membrane fusion with stable conformational modification [4]. This essential entry process is an important target for antibody mediated neutralization.

SARS-CoV-2 S protein holds 98% sequence similarity with the bat coronavirus RaTG13. A most critical variation observed in CoV-2 due to an insertion "RRAR" furin recognition site at S1/S2 junction, while SARS-CoV-1has single arginine at that site. Besides this insertion, ~60% residual substitutions are noted at the RBD domains [5]. Revealing how such differences contribute to higher recognition capability of hACE2 receptor is important to underpin the therapeutic target that can prevent virus entry. Here, we have analysed respective protomers of four S-protein cryo-EM structures: SARS-CoV-1 (pdb id: 6CRZ) [6], SARS-COV-2 (pdb id: 6VYB) [4] (Fig.1), SARS-CoV-RBD-hACE2 complex (pdb id: 2AJF) [7], and SARS-CoV-2-RBD-hACE2 complex (pdb id: 6M17) [8]. These analyses revealed that SARS-COV-2 and SARS-CoV-1with the RBD of up-conformational form can only bind with hACE2. Relative to this up-form CoV-RBD, CoV-2-RBD has expanded its net surface area, with large local conformational changes of AA resides, higher RMSD of Cα atoms and relatively large amplitude anti-phase-like RBD motion in the slow-motion second normal mode. It has further been shown that much closer interactions between CoV-2-RBD and hACE2 are resulted in significant loss of structural rigidity, triggering proteolytic processing of S protein for membrane fusion.

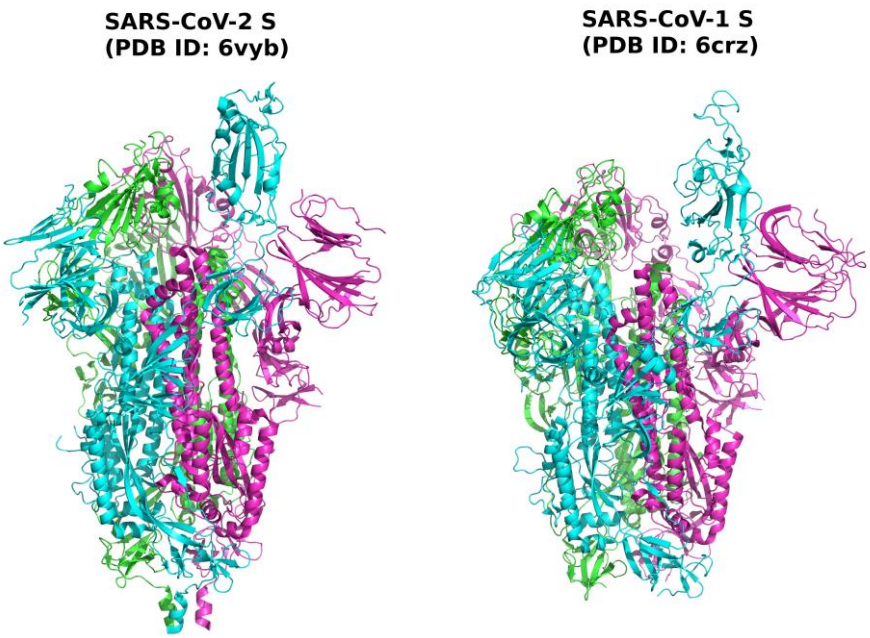

Fig.1 Spike (S) glycoprotein of SARS-CoV-1 and 2; It is a trimer (represented with three different colours) protruded from virion surface and responsible for the receptor recognition and membrane fusion. Here, both the spike proteins have retained one of the monomers with the receptor-binding domain (RBD) of up-conformational form (cyan colour) which can only bind with the human receptor hACE2.

Results

High variability of the receptor-binding domain (RBD)

Coronavirus (CoV) spike glycoprotein (S protein) protruded from virion surface is responsible for the receptor recognition and membrane fusion, which are essential steps for viral entry into the host cell [9]. The S1 unit of S protein contributes to receptor recognition and priming of S2 unit for membrane fusion. In order to recognize host receptor, the receptor-binding domain (RBD) of S1 undergoes hinge-like conformational motions. In a recently reported structure of SARS-CoV-2, it has observed that human angiotensin-converting enzyme 2(hACE2) can only bind with the RBD (residues 336-518) having up-conformational state. Peptidase domain (PD) of hACE2 clashes when all the RBD domains of the homotrimer SARS-CoV-2 S are in down conformational state. To identify characteristic differences between the up-RBD of SARS-CoV-1and CoV-2, we superimpose both the structures with and without the binding of hACE2 (Fig.1A). Despite a number of sequence variations, structural alignments show overall similarities (Fig.2A) in most portions. However, RBD AA residues showed ~2 fold higher root mean squared deviation (RMSD) from the average level of ~2.0 Å. In contrast, bound RBD have a very high RMSD variation (Fig.2B) and shows lower than the average value for many residues. Moreover, we have plotted Ramachandran plot for bound-RBD in both the complex. It displays large changes in phi and psi dihedral angles for most of the RBD residues in favourable and allowed regions of the plot (Fig.4B). All together, these results indicate characteristic conformational differences in hACE2-bound and non-bound RBD between SARS-CoV-1and SARS-CoV-2.

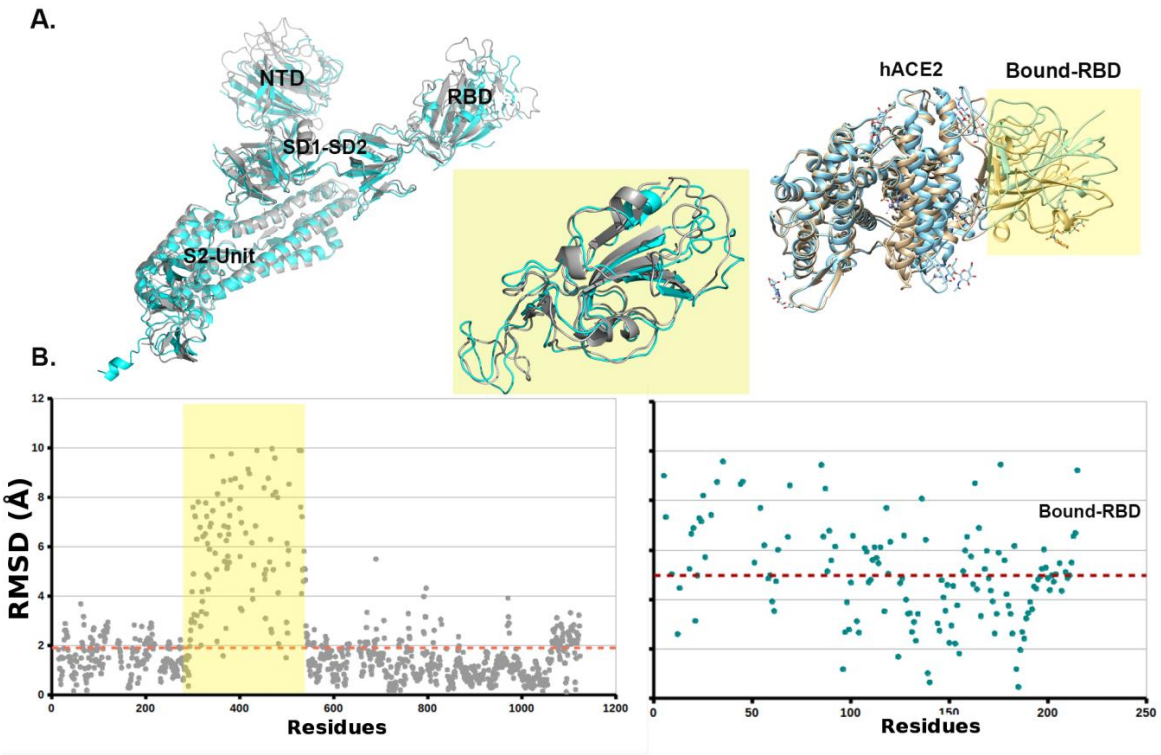

Fig.2. **Root-mean-squared deviation (RMSD) of Cα atoms. (A)** We used MatchMaker in UCSF-Chimera to superimpose structures. It considers similar structures to be superimposed while there are large sequence dissimilarities by producing residue pairing with the inputs of AA sequences and secondary structural elements. After superposition, it uses the usual Euclidian distance formula for calculating RMSD in angstrom unit. (B) Left side graph shows RMSD between the structures SARS-CoV-1(PDB id: 6CRZ) and CoV-2-RBD (pdb id: 6VYB) up-conformation protomer, while the right side graph shows RMSD of hACE2-bound RBD between SARS-CoV-1-RBD-hACE2 (2AJF) and SARS-CoV-2-RBD-hACE2 (6M17) complex. Yellow-shaded region shows relatively high deviations in the receptor-binding domain (RBD).

Differential RBD motions between CoVs

Significant conformational changes are commonly reflected in the differential domain motions. To capture such differences, we have conducted normal mode analysis using combine approaches of Gaussian network model (GNM) and anisotropic-network model (ANM) in DynOmics webserver and in iMODS (http://imods.chaconlab.org). This hybrid model has efficiently captured the dynamic differences between SARS-CoV-1and SARS-CoV-2 with and without hACE2 bound. With the trimeric CoV-1and CoV-2 macromolecular structure, we have calculated covariance matrix in the iMODS webserver which is computed using the $C\alpha$ Cartesian coordinates and the Karplus equation of collective motion in protein. This covariance matrix signifies coupling between pairs of residues (Fig.3A,B). Overall, covariance patterns are very similar for CoV-1and CoV-2; however, there are few sharp differences in few spots of the covariance matrices.

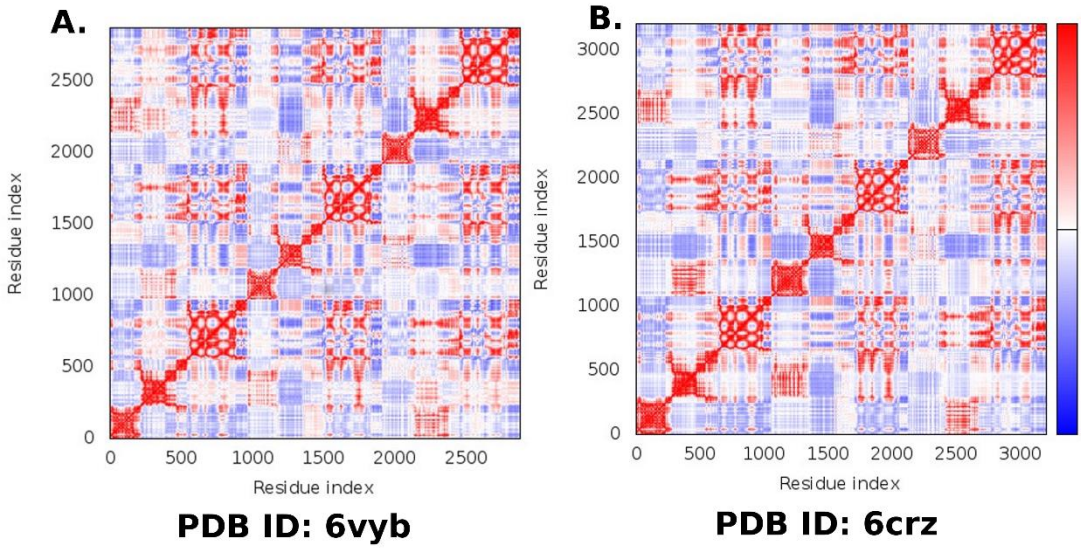

Fig.3. Coupling between pairs of residues-a covariance matrix with positively correlated (red), uncorrelated (white) or anti-correlated (blue) motions (prepared in iMODS webserver http://imods.chaconlab.org)

As usual, such differences are prominent in the low-frequency normal modes. To examine the internal residual coupling and its effects, we have studied low-frequency normal modes for RBD-up monomer of both the structures and noted that the second normal mode capable to effectively capturing these differences. It shows that RBD has relatively high amplitude motions for both the CoVs without hACE2 binding, while the S2-unit holds lower-amplitude motions (Fig. 4A). When we compare this prefusion up-form RBD local motion along the residues of CoV-1and CoV-2, it shows that the extended RBD region follows anti-phase like dynamics; CoV-2-RBD has positive eigenvectors in oppose to negative eigenvectors of CoV-1-RBD (Fig.4D). In contrast, these anti-phase dynamics are mostly vanished due to hACE2 binding. hACE2 binding makes the RBD relatively stable, with little faster movements of CoV-2-RBD (Fig.4A, C).

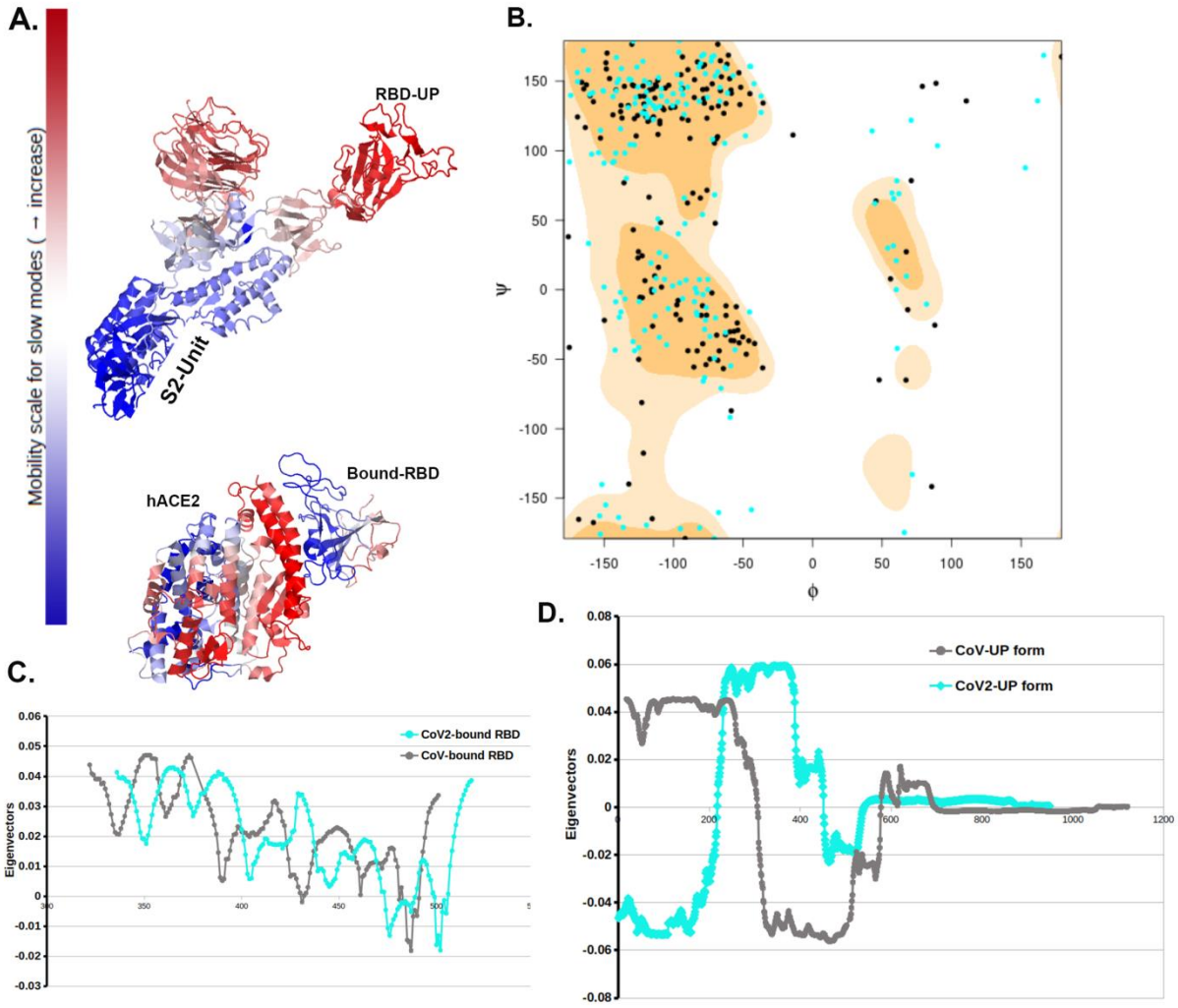

Fig.4.**Normal Mode Analysis (NMA) and Ramachandran plot.** We used low-frequency second normal mode to differentiate between SARS-CoV-1 and SARS-CoV-2 with and without hACE binding. (A) Its RBD-up conformation region in the S1-unit has higher mobility relative to other parts of the S-protein. In contrast, hACE2 binding make the RBD less mobile. (B) Ramachandran plot of AA residues of RBD bound with hACE2. Cyan dots represent CoV-2-RBD AA residue phi-psi position, while black is for CoV-1complex. It shows significant conformational changes in the RBD. (C) Residue-wise eigenvectors of bound RBD AA residues is representing low-frequency motions. There are no significant differences in bound RBD motions between both the SARS-CoV-1complexes. (D) Without hACE binding, RBD up-conformation protomer is showing significant differences in the domain motion in the RBD regions. It is like anti-phase-type dynamics between the two CoVs structures.

Two representative conformational states for each SARS-CoV-1 and SARS-CoV-2 were considered for the analysis of dynamical features: the whole spike protein with one RBD in the open state and the single RBD domain bound to the ACE2. The Figure S1 and the Figure 5 illustrate initial conformations of SARS-CoV-1 and SARS-CoV-2 spike protein with one RBD in the up state. The Figure S1 shows the side and top views of both spike proteins, with RBD up in front, with RBD-up are the most at the bottom. In these figures different colored domains represent different chains. The domain in green represent chain A, the domain in cyan chain B

and in magenta chain C. For the SARS-CoV-1 case, RBD in the up state belongs to the chain A, whereas the SARS-CoV-2 the up state is in the chain B.

Figure 5A, B represent the ensemble of superimposed snapshots produced by FRODAN for both spike proteins at energy cut-off -1.0 kcal/mol. This representation qualitatively gives impression about the sampled conformational space by individual protein domains. Various fluctuation scales are present in SARS-CoV-1 and SARS-CoV-2 spike protein. The largest fluctuations in both exhibit the RBD that is in the up state. While comparing both spike proteins, stronger fluctuations exhibit SARS-CoV-1. Fluctuation magnitude in each domain can be explicitly measured by the RMSF of the respective backbone atoms. The Figure 5A, B reveals RMSF fluctuations in both spike proteins at different energy cut-offs (temperatures). Consistently with normal mode analysis it is evident that for both spike proteins the RBD in the up conformation has higher fluctuation magnitude if compared to other domains including RBDs in the down state at all considered cut-off values. Overall the changes in the RMSF profile with the change of the temperature are more pronounced for the SARS-CoV-1 rather than for the SARS-CoV-2 (Table S3, S4). For the SARS-CoV-1 the reduction of energy cut-off from 0.0 to -2.0 kcal/mol results in increase of average RMSF across all domains from 4.2±2.2Å to 9.2±6.6Å. Whereas for SARS-CoV-2 the energy cut-off reduction leads to relatively small increase from 5.1±4.3Å to 6.1±4.3Å. Interestingly, the SARS-CoV-1 spike protein's RBD in the up state at lower energy cut-offs: -0.0 and -0.1 kcal/mol exhibit lower fluctuation magnitude compared to the one in SARS-CoV-2: 7.8±2.8Å vs 17.8±8.0Å at -0.0 kcal/mol and 11.9±4.1Å vs 19.5±8.8Å at -0.1 kcal/mol respectively. Contrary to that at higher energy cut-offs: -1.0 and -2.0 kcal/mol fluctuation magnitude of the RBD in the up state is higher in the spike protein of SARS-CoV-1rather than in the case of SARS-CoV-2: 25.1±9.0Å vs 18.0±7.9Å and 27.9±9.9Å vs 16.4±6.8Å. These observations are in partial agreement with [11], where SARS-CoV-1 exhibited stronger fluctuations than SARS-CoV-2 at the room temperature. Overall it seems that temperature increase affects the SARS-CoV-1spike protein in the more pronounced way than the spike protein of SARS-CoV-2. This may point out on the higher stability of ACE2 binding competent state of the SARS-CoV-2. This finding confirms also general trend of higher sensitivity to meteorological conditions of SARS-CoV-1 in comparison to SARS-CoV-2 [12-13].

Figure 5C,D compare the ensemble of snapshots for SARS-CoV-1and SARS-CoV-2 complexed with RBD at energy cut-off -1 kcal/mol. Overall ACE2 bound with SARS-CoV-1fluctuates in the similar manner to the ACE2 bound with SARS-CoV-2. Nevertheless, RBD domain of SARS-CoV-1 bound to ACE2 seems to have larger fluctuation amplitude comparing to the RBD of SARS-CoV-2 in the bound state. These features are reflected in the corresponding RMSF profiles of ACE2 and RBD in each complex at different energy cut-offs, summarized in the Figure 5C, D and Table S4. Consistently with visual observations with the energy cut-off reduction ACE2 fluctuation magnitude increases in similar manner in both complexes, no substantial differences are observed. The change of energy cut-off from 0.0 to -2.0 kcal/mol leads to the change of average RMSF of ACE2 complexed with SARS-CoV-1from 2.9±1.0Å to 4.4±1.4Å and for ACE2 complexed with SARS-CoV-2 from 3.0±1.0Å to 4.3±1.4. Whereas RBD domain dynamics in the complex overall is less mobile for the SARS-CoV-2 case rather than for the SARS-CoV-1. Average RMSF of the former one is lower at all considered cut-offs. With energy cut-off reduction average RMSF of SARS-CoV-1RBD complexed with ACE2 changes from 4.3±1.9Å to 7.0±2.9Å, whereas in case of SARS-CoV-2 the change is from 4.0±1.7Å to 5.5±2.3Å. Which points out on the stronger contacts in the complex between ACE2 and SARS-CoV-2. This result correlates with higher binding affinity as well as infectivity of the SARS-CoV-2 if compared to SARS-CoV-1[12-14].

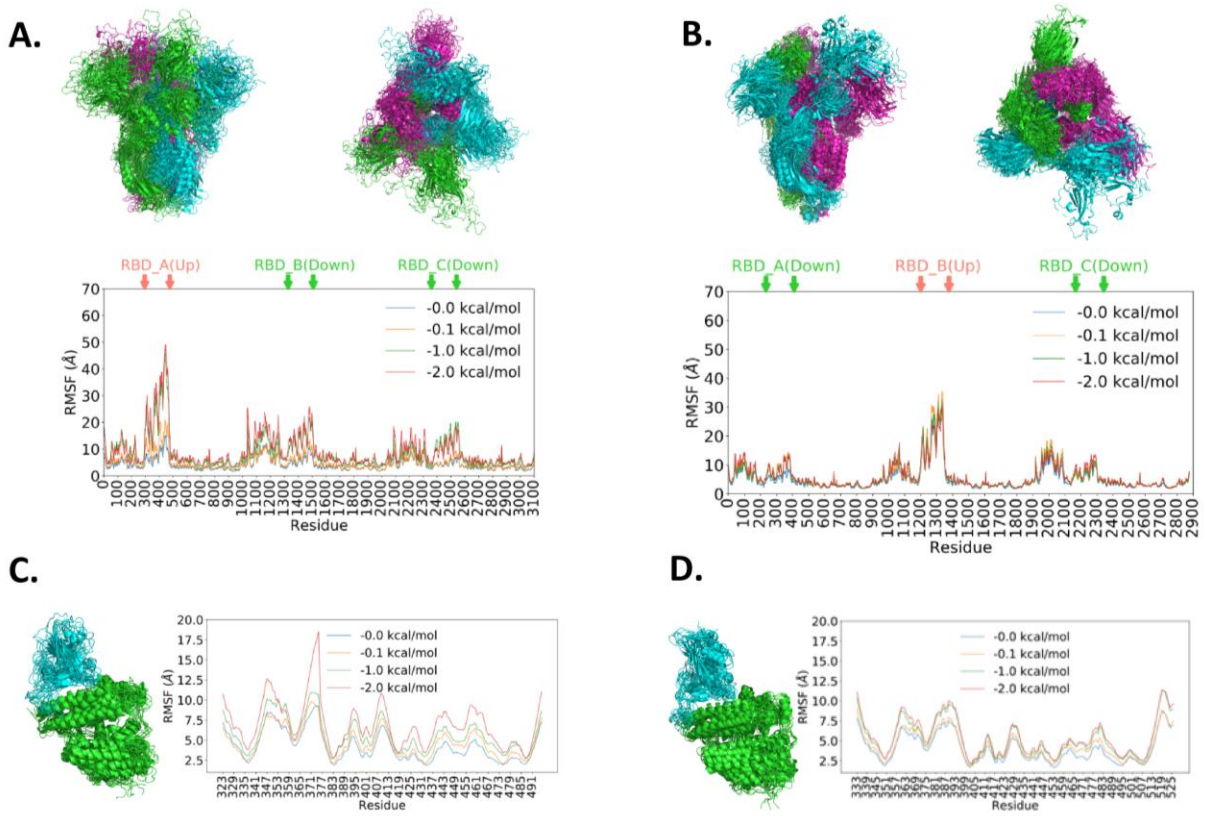

Fig.5 Ensemble of spike conformations with FRODAN v1.0.1 [10]**:** (A, B) SARS-CoV-1 and SARS-CoV-2 with Fluctuation magnitude in each domain explicitly measured by the RMSF of the respective backbone atoms, (C,D) RMSF of RBD-UP domain bound with ACE2, showing lower fluctuations in SARS-CoC-2 bound RBD.

Uneven distribution of interface molecular interactions between the RBD and hACE2

Interface interactions certainly play crucial role for binding and that of dynamic domain separation shown in normal mode analysis. Here, we use Prodigy webserver to predict these interactions [15]. Interface between CoV-2-RBD and hACE2 is relatively higher than the SARS-CoV-1complex, with higher potential for large intermolecular interactions. Although both the complexes hold almost similar binding affinity for the hACE2, there are slight observable differences in dissociation coefficient (i.e. 7.3 nM for CoV-RBD-hACE2 complex and 12 nM for CoV-2-RBD-hACE2) (Table 1). This noted difference may arise due to differential interface molecular interactions (Table S1 and S2). In both the complexes, almost all interface molecular interactions involve loops and small parts of beta-sheets secondary structures of RBD and a single alpha helical structure of hACE2, indicating interface instability (Fig.4). We find uneven distribution of interface interactions along this single hACE2 alpha-helix. While two end portions and the middle part of the helix hold most interactions, there are lot more differences of interacting residues between CoV-1and CoV-2 complex (Table S1). In particular, we note that hACE2.GLU35[OE2]–RBD.GLN493[NE2] and hACE2.THR27[O] – RBD.TYR489[OH] come closer (~2.6 Å) and form H-bonds in the CoV-2-RBD-hACE2 complex (Fig.6). Inclusion of these two additional polar interactions may affect subsequent proteolytic processing of S protein and membrane fusion with the S2-unit.

Table 1: Interactions between hACE2 and the coronavirus Receptor-binding Domain (RBD)

Complex name (PDB ids)	Bound-RBD surface area (Å^2)	Interface Area (Å^2)	Binding Affnity (kcal/mol)	Dissociation constant (nM)	Polar-polar contacts added	LJ interactions with water (kcal/mol)	Coulomb inter-actions with water (kcal/mol)
SARS-CoV-RBD-hACE2 (2AJF)	18435.672	796.7	-11.1	7.3	2	-281	-4887
SARS-CoV2-RBD-hACE2 (6M17)	19866.404	827.7	-10.8	12	2+2; added GLU35 – GLN493 THR27 – TYR489	-261	-5160

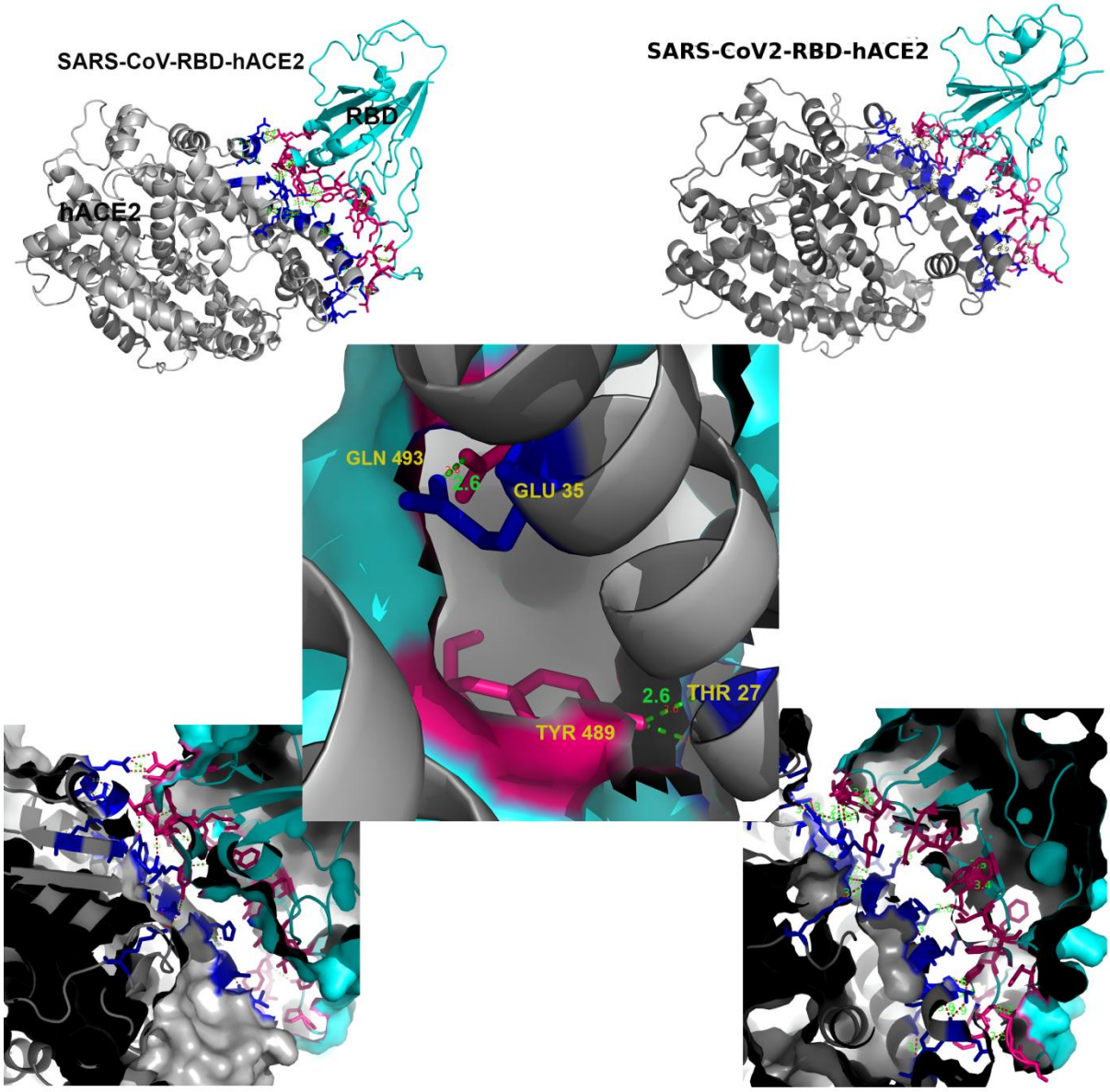

Fig.6. Interface interactions between CoV-1receptor-binding domain (RBD) and the human receptor membrane protein hACE2. In both the complexes, almost all interface molecular interactions involve loops and small parts

of beta-sheets secondary structures of RBD and a single alpha helical structure of hACE2. We note that hACE2.GLU35–RBD.GLN493 and hACE2.THR27 – RBD.TYR489 (~2.6 Å) forms H-bond interactions in the CoV2-RBD-hACE2 complex.

In order to check reliability of predicted interface interactions, we have calculated ^{13}C chemical shifts (δ) using structural coordinates of both the CoV-1and CoV-2 hACE2 bound complex. This calculation is carried out using SHIFTX2 that combines ensemble machine learning approaches with the sequence alignment-based methods and that has carefully been trained with 197 high-resolution protein structures. We note that there is no overall significant differences in δ (ppm) between the hACE2 bound CoV-1and CoV-2 complex (Fig.7A). However, relative absolute differences in δ ($\Delta\delta$) are prominent at the interface between hACE2 and RBD (Fig.7A middle). Detected uneven distribution and changes of interface interactions are shown to be strongly correlated to deviation in the chemical shifts ($\Delta\delta$). In particular, the hACE2 interface helix and the interacting RBD domain of the CoV-2 RBD shows significant difference in $\Delta\delta$ (Fig.7B). As expected, very high $\Delta\delta$ values are noted at and nearby H-bond forming residues GLU 35, THR 27 on the hACE2 helices and GLN 493 and TYR 489 on the RBD interface (Fig.7B). A large $\Delta\delta$ pick of 14.86 ppm on the RBD-interface and 2.50 ppm on the hACE2 helix are noted, with significant changes in the middle and end parts of the interacting interface helix. Furthermore, large picks in $\Delta\delta$ corresponds to AA substitutions. For example, $\Delta\delta$ pick of 14.86 and 8.90 ppm correspond to the substitution THR433GLY446 and THR487ASN501 on the interacting RBD domain.

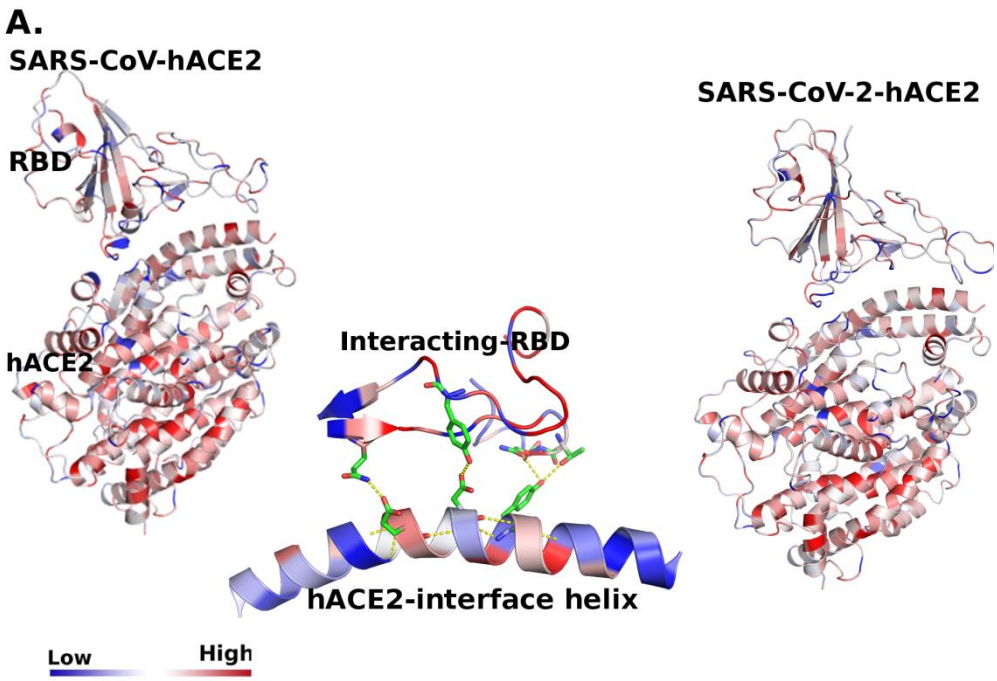

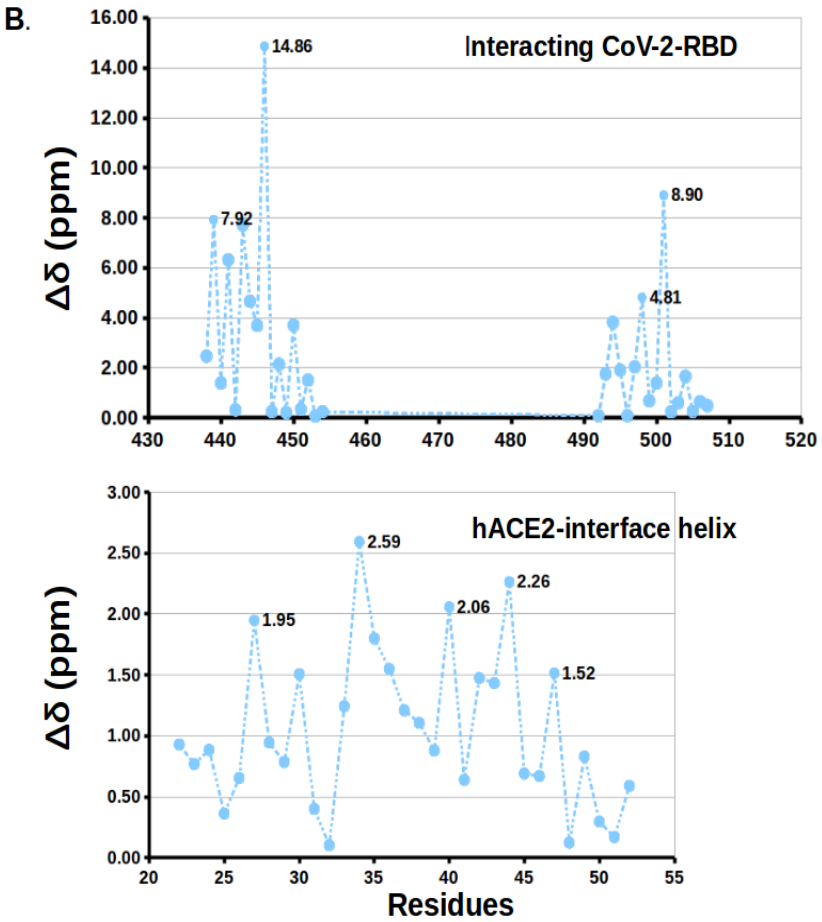

Fig.7. ^{13}C Chemical shifts (δ) and changes in ^{13}C chemical shifts ($\Delta\delta$) indicate the changes in the interface interactions between hACE2 and RBD. (A) there are no overall significant differences in δ (ppm) between the hACE2 bound CoV-1and CoV-2 complex (top two figures), the middle figure shows the deviation in chemical shifts ($\Delta\delta$) at the interface interacting sites, (B) A large change in $\Delta\delta$ are observed at and nearby H-bond forming residues GLU 35, THR 27 on the hACE2 helices and GLN 493 and TYR 489 on the RBD interface.

hACE2 binding induces changes in structural flexibilities

How hACE2 binding promote membrane fusion is critical to understand virus entry into host cell. As mentioned above that hACE2 binding triggers local conformational changes and how such changes alter structural flexibilities underpin effective membrane fusion. To address this question, we have carried out rigidity analysis using Floppy Inclusion and Rigid Substructure Topography (FIRST) program [16] which is based on pebble game algorithm and techniques in rigidity theory. FIRST decomposes the protein structure into multiple rigid clusters with the input of H-bond energy cutoff (H-cut-off). With H-cut-off of 0.00, -0.5, -0.1 and -1.5, both the complexes have been decomposed into several rigid clusters. As H-cut-off increases, number of rigid cluster is elevated with decreasing size. Given all the H-cut-off, no significant differences are observed for CoV-1and CoV-2 up-form RBD. However, hACE2 bound complexes show differences in number, size and distribution of rigid clusters between CoV-1and CoV2-RBD-hACE2 complex (Fig.8 and Table 2). Upon hACE2 binding, it shows that CoV-2 complex becomes highly flexible which favours proteolytic processing for membrane fusions.

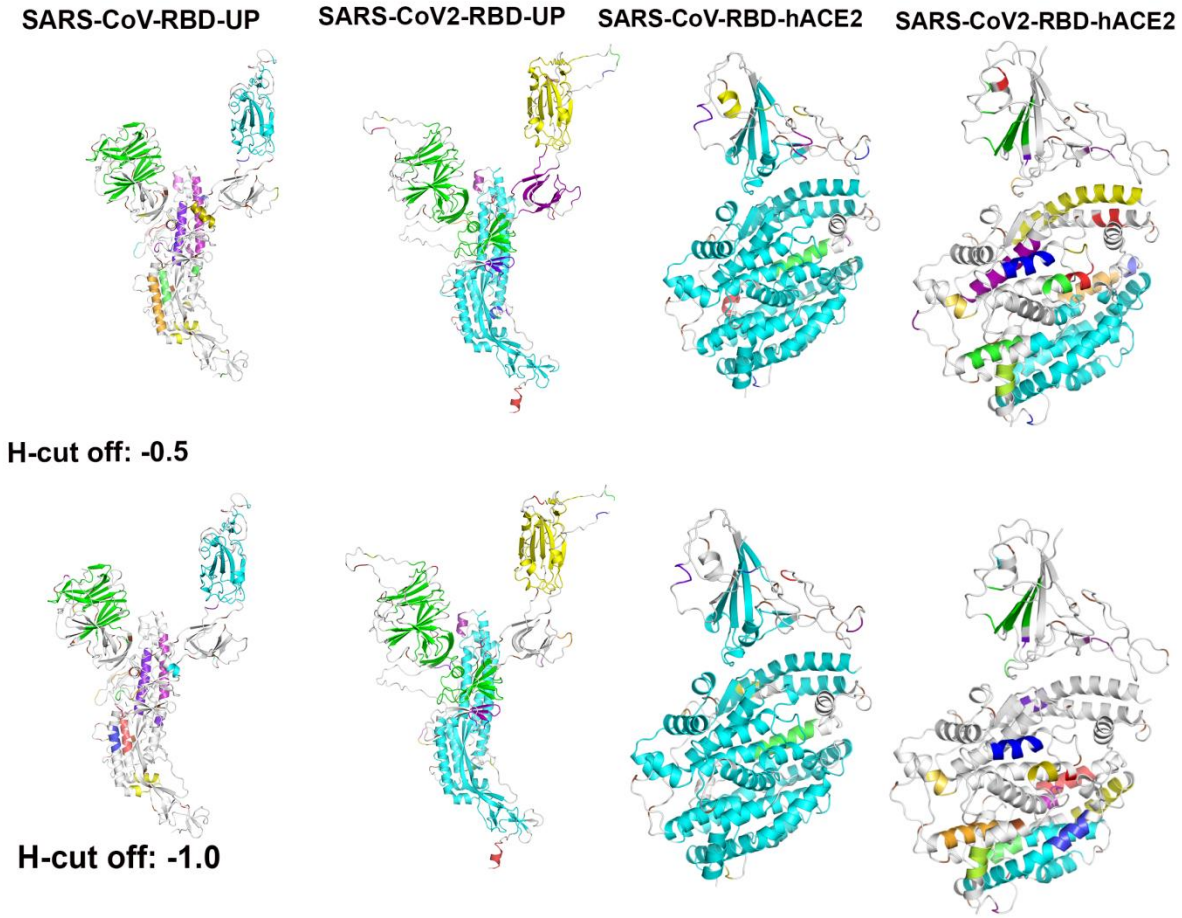

Fig.8. **Rigidity analysis of protein structures**. With H-bond energy cut-off -0.5, -0.1, all the four protein structures have been decomposed into several rigid clusters. Coloured region shows rigid cluster. Although there is no significant differences between SARS-CoV-1and SARS-CoV-2, hACE2 binding in the SARS-CoV-2-RBD makes the structure more flexible with less number and smaller size of rigid clusters.

Table 2: Residues rigid clusters for bound hACE2 and RBD domain

H-bond cutoff	SARS-COV-RBD-hACE2		SARS-COV2-RBD-hACE2	
	hACE2	Bound RBD	hACE2	Bound RBD
H-cutoff: 0.0	22-84, 98-101, 148-255, 262-284, 294-333, 346-423,432-489, 500-574, 581-598	340-344, 383-397,419-440, 479-500,	109-112, 115-129, 152-204, 218-247, 262-265,270-271, 450-489, 498-518	No significant rigid cluster
H-cutoff: -0.5	22-80, 158-209, 217-255, 262-284,294-333, 346-360, 366-423,432-489, 500-531, 539-574,581-598	340-344, 383-397,420-440, 479-500	158-204, 218-247,262-265,270-271, 450-489, 498-517, 582-585	No significant rigid cluster
H-cutoff: -1.0	22-52, 67-80, 158-171, 177-209, 217-255, 262-284,294-317, 323-333, 346-360,366-385, 389-423, 432-489,500-	340-344, 383-397,420-440, 479-500	230-247, 450-464,473-489,	No significant rigid cluster

	531, 539-574, 581-597			
H-cutoff:-1.5	23-51, 67-80, 157-170, 177-191, 223-255, 262-284,294-317, 323-333, 346-360,366-385, 389-423, 432-464,473-489, 500-531, 539-558,581-597	No significant rigid cluster	No largest rigid cluster found	No significant rigid cluster

Interfacial water promotes and stabilizes the formation of CoV-2/hACE2 complex

Previous studies [17,18] have indicated that water-mediated interactions can play an essential role in stabilization of CoV/hACE2 complex. It can be shown [18] that a gap between the RBD/hACE2 protein-protein complex includes several hundred interfacial water molecules which can form bridges between amino acids of the RBD and hACE2 subunits. Using the three-dimensional reference interaction model (3D-RISM) approach (see details in Methods) we have evaluated this phenomenon and calculated a distribution of interfacial water and its probable influence on the complex formation. Figure 9a demonstrates a water distribution in the interfacial region for CoV-2/hACE2 complex. Water molecules are depicted only in the most probable positions. As it is seen, the interfacial water interacts strongly with the RBD as well as with the hACE2 subunits, the latter confirms the previous molecular dynamic simulations [18]. However, our calculations yield the water-mediated interactions to be stronger for the CoV-2/hACE2 complex than those for the CoV/hACE2. See for example Fig. 9b demonstrating a relative difference in distributions of water oxygens (blue) and hydrogens (red) between the two complexes. Moreover, the water interacts more strongly for CoV-2/hACE2 rather than for pure coronavirus. This effect is also confirmed by the calculations of water-complex interaction energies (Table 1). The data on interaction energies between the complexes and interfacial water proves this fact. Although the Lennard-Jones energy between the CoV/hACE2 and water is stronger than that for the CoV-2/hACE2 complex, the total interaction energy has a more profit for the latter complex due to a strong decrease in the electrostatic energy. This observed effect can be explained by a polarization of interfacial water which is stronger for the CoV-2/hACE2 complex.

Apart from it, the latter complex forms water bridges whose number is larger by 2 than in the case of CoV/hACE2. At the same time the water bridges is more stronger in the CoV-2/hACE2 aggregate. For example, we have calculated the potential of mean force (pmf) between atoms of corona virus and hACE2 receptor (Fig. 10). It is clearly seen that bridging water molecule forms simultaneously hydrogen bonds with CoV-2 (Gln493) and hACE2 (Glu35) amino acids in the case of CoV-2 (Figs. 10a and 10c). However, the similar hydrogen bond with bridging water is very weak and diffusive for the CoV/hACE2 complex (Figs. 10b and 10d). Therefore, we conclude that bridge water molecules play a significant and, perhaps, crucial role in stabilizing CoV-2/hACE2 complex.

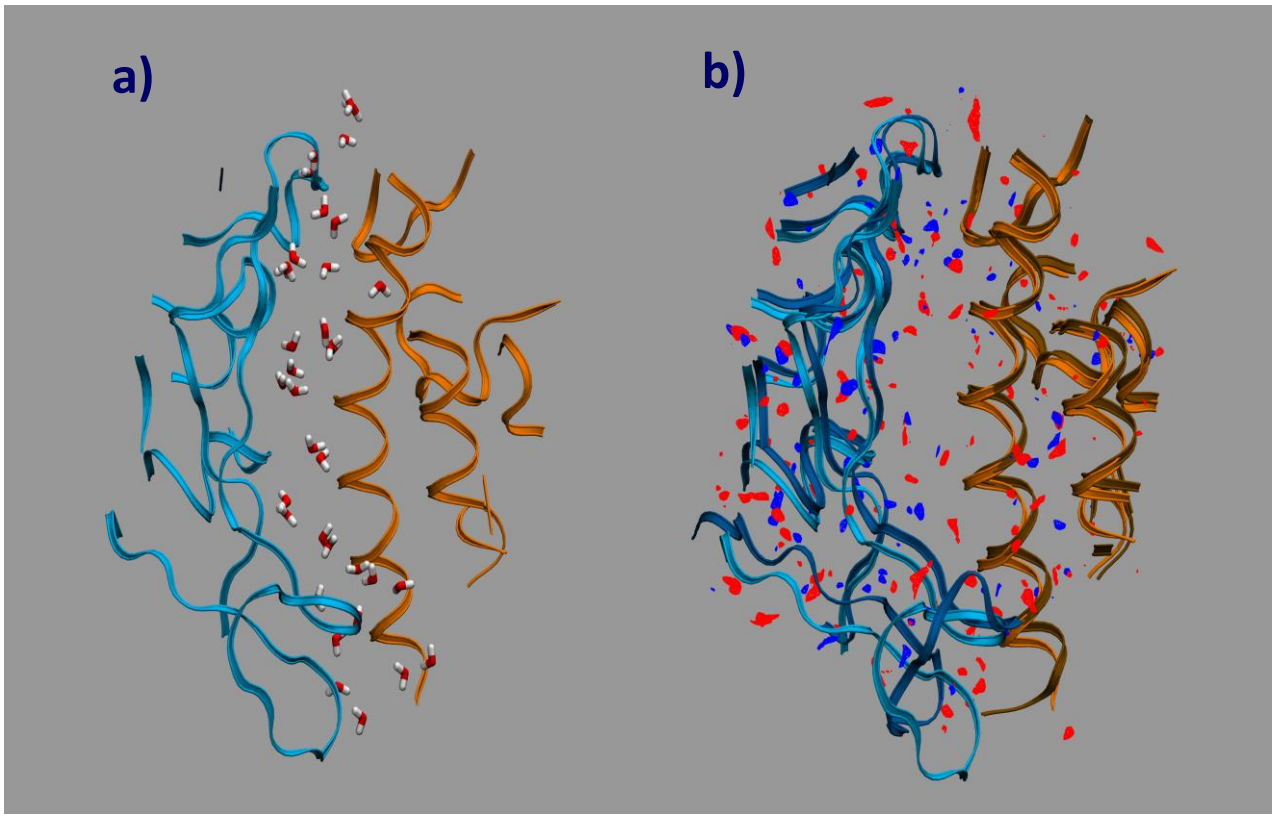

Fig.9. Water distribution in the interfacial region of complexes: a) for the CoV-2/hACE2 complex, b) differences in distributions of water oxygens (blue colour) and water hydrogens (red colour) between the CoV-2/hACE2 and CoV/hACE2 complexes. The RBD is indicated by blue ribbons, the hACE2 by orange ribbons, and the CoV/hACE2 is shown as background for the differences.

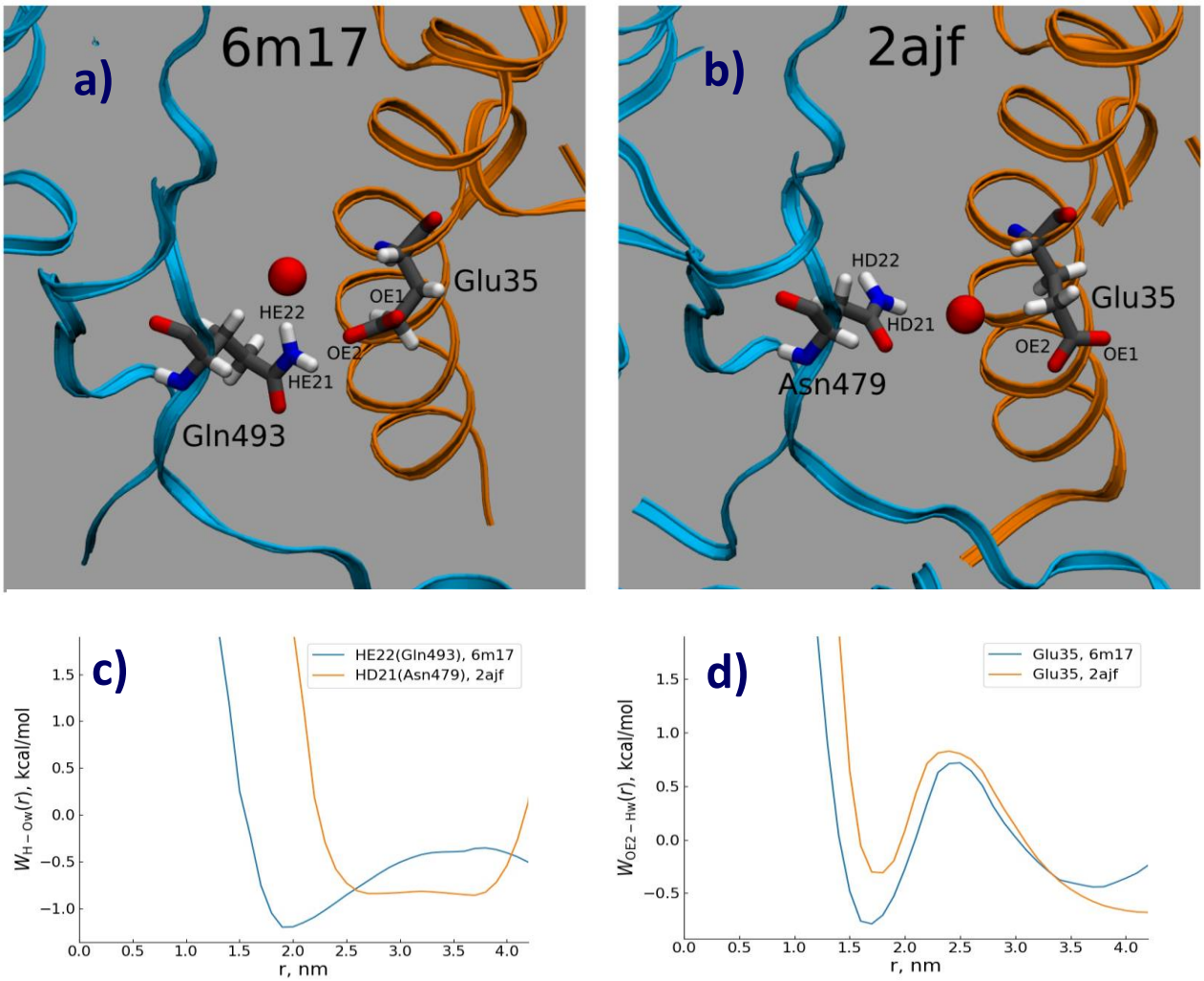

Fig.10. Water bridging the complexes: a) location of water oxygen bridging the CoV-2/hACE2 complex, b) the same for the CoV/hACE2 complex, c) the pmf of H-O distribution for the CoV-2 and CoV-water bridges, and d) the pmf of O-H for the hACE2-water bridges in the complexes.

Conclusions

Viral entry into host cell, subsequent replication and transmibility are essentially dependent on receptor recognition, binding, and membrane fusion mechanisms. SARS-coronavirus use ectodomain trimer, spike glycoprotein (S-protein), to mediate this viral entry [19]. Both SARS-CoV-1and SARS-CoV-2 recognizes the human membrane receptor protein hACE2 through its receptor-binding domain (RBD) positioned within the flexible S1 unit of S-protein protomer. S-protomer with the RBD up-conformational forms can only recognize hACE2. With down RBD conformations in all the three protomers of S-protein prevent hACE2 binding. Prefusion RBD conformation is, therefore, very important to determine receptor binding and thereby its differences between CoV-1and CoV2 underpin the higher success of human-to-human transmission of SARS-CoV2. Understanding prefusion conformation and receptor binding and its differences among closely related species are critical for designing vaccine and inhibitors to strop viral entry. For example, one recent structural study has tested multiple SARS-CoV-1RBD specific monoclonal antibodies and found that none of them have notable binding to CoV-2 RBD [5]. Recent major therapeutic efforts are targeting the interactions between the SARS-CoV-2 spike (S) glycoprotein and the human cellular receptor angiotensin-converting enzyme, hACE2 [20-22]. It has recently been demonstrated that SARS-CoV-1S murine polyclonal antibodies can potentially inhibit SARS-CoV2 S mediated viral entry. However, its underlying inhibition mechanism is poorly understood [4].

Using recently reported cryo-EM structures of SARS-CoV-1and CoV-2 S protein we find effective conformational differences in the RBDs at prefusion state. With higher surface area of CoV-2 RBD and large local conformational changes in the AA residues, it establishes higher interactions with the human receptor hACE2. These underlying conformational differences are illustrated with the higher RMSD of Cα atoms, changes in phi and psi dihedral angles and relatively large amplitude anti-phase-like RBD motion. In particular, we note that hACE2.GLU35–RBD.GLN493 and hACE2.THR27 – RBD.TYR489 come closer in the CoV2-RBD-hACE2 complex and forms important H-bonds. However, it remains to be explored how efficiently CoV-2 regulate and open-up RBD for hACE2-binding. The RBD of CoV-2 forms more number and more stronger water bridges with the hACE2, and the letter play a significant role in the total stabilization of the CoV-2/hACE2 complex. Inclusion of the two noted additional polar interactions affects structural flexibilities. We find such interaction changes critically affect structural flexibility. In particular, hACE2 binding makes the CoV-2 structure more flexible relative to CoV-1complex. This h-ACE2-induced structural flexibility favours subsequent proteolytic processing which is essential for membrane fusion. This understanding certainly provides a clue for designing novel vaccine and antiviral drugs.

Methods

Root-mean-squared deviation (RMSD) of Cα atoms

We used MatchMaker in UCSF-Chimera to superimpose structures. It performs a best fit after automatically identifying pair of residues. It considers similar structures to be superimposed while there are large sequence dissimilarities by producing residue pairing uses with the inputs of AA sequences and secondary structural elements. After superposition, it uses the usual Euclidian distance formula for calculating RMSD in angstrom unit with the use of PDB atomic coordinates files.

Normal Mode Analysis (NMA)

DynOmics ENM Server [23] was used to perform normal mode analysis (NMA). NMA is a well-explored technique for exploring functional motions of proteins. It combines two elastic network models (ENMs) — the Gaussian Network Model (GNM) and the Anisotropic Network Model (ANM) to evaluate the dynamics of structurally resolved systems, from individual molecules to large complexes and assemblies, in the context of their physiological environment. In the GNM model, network nodes are the C-alpha atoms and the elastic springs represented the interactions. We used GNM with interaction cut-off distance of 7.3 Å and spring constant scaling factor cut-off of 1 Å for the calculation of the elastic network model. We calculated the first twenty slowest modes for all the CoVs structures. The eigenvectors of these modes represent the global motions and the constrained residues help in identifying critical regions such as hinge-bending regions and thereby giving an idea of domain motions around these regions. We plotted the second slowest mode in different conditions which showed a significant difference in motions.

Constrained geometric simulations for conformational sampling

To study dynamics of the considered structures, we employed a low computational complexity alternative to MD geometric molecular simulation package FRODAN v1.0.1 [10]. We run FRODAN in the non-targeted mode, generating 30,000 candidate structures for each case. The temperature impact was evaluated by running simulations at different hydrogen bond energy cut-offs. The considered range of the energy cut-offs was from 0.0 to -2.0 kcal/mol, with that of the more negative cut-off values correspond to higher temperature. During each individual run the cut-off value was kept constant. Before running simulations, hydrogen bonds to each considered structure were added using MolProbity server:
(http://molprobity.biochem.duke.edu/).

Rigidity analysis

We use the program Floppy Inclusion and Rigid Substructure Topography (FIRST) [16] that generates a constraints network from the coordinates of the protein structure in terms of nodes (atoms) and edges (covalent bonds, hydrogen bonds and hydrophobic interactions). Hydrogen bonds were ranked according to their energy strength using Mayo potential, whereas the value of energy strength was selected in such way that the bonds strength below this cut off were ignored. First then applies the rigorous mathematical theory of rigid and flexible molecular structure and pebble game algorithm calculates the degree of freedom of motion to rapidly decompose a protein into rigid clusters and flexible region.

3D RISM calculations

The 3D- RISM method [24-25] with the 3D-Kovalenko-Hirata closure was used to describe hydration of CoV-2/hACE2 and CoV/hACE2 complexes. These calculations describe hydration on a molecular-atom level and has proven their power in many successful studies of ion / molecule hydration, including various biocompounds [26-36]. In the framework of 3D-RISM theory molecule-atom spatial distribution functions are obtained. These functions are the 3D-site distribution functions of water atoms around the complex. The RISM-calculations were carried out for the studied complexes hydrated in water at ambient conditions. For water the modified version of the SPC/E model (MSPC/E) was used [37]. The corresponding LJ parameters of the solute atoms were taken from the ff14SB force fields [38]. The 3D-RISM calculations were performed using the rism3d.snglpnt codes from the AmberTools 16 package [39]. The 3D-RISM equations were solved on a 3D-grid of 350 × 320 × 350 points with a spacing of 0.025 nm. A residual tolerance of 10^{-6} was chosen. These parameters are enough to accommodate the complex together with sufficient solvation space around it so that the obtained results are without significant numerical errors.

Acknowledgments

Our thanks to our lab members, Sikkim University for their support while completing a part of computational study in this work. This research was supported by SERB-EMR grant (file no. EMR/2015/001671). The study of ChGN was supported by the Government Contract of the Institute of Theoretical and Experimental Biophysics, Russian Academy of Sciences (N 075-00381-21-00). The study of MVF and SEK was performed under the Government Contract of G.A. Krestov Institute of Solution Chemistry, Russian Academy of Sciences (N 0077-2019-0033).

Author Contributions

NK, SB, MR, AC have designed the study and conducted computational experiments and analytical analysis. AS, KS, AT carried out residual analysis based on PDB files and has written the corresponding part. GC, MF, SEK has formulated the problem of hydration for COVID-hACE2 complex, performed the initial calculations and written the corresponding section of the paper. SEK has performed all 3D-RISM calculations and a visualization of the results. MVF has conducted a formal analysis and discussion of 3D-RISM results and written the corresponding section of the paper. GC, AS, and AC have reviewed and written the article.

Declaration of Interests

The authors declare no conflict of interest.

References

1. Kucharski AJ, Russell TW, Diamond C, Liu Y, Edmunds J, Funk S, Eggo RM. 2020 Early dynamics of transmission and control of COVID-19: a mathematical modelling study. *Lancet Infect Dis* 20: 553-558.

2. Zhu et al.2020.A novel coronavirus from patients with pneumonia in China, 2019 *N. Engl. J. Med.* 382: 727-733 (doi: 10.1056/NEJMoa2001017).

3. Qing E, Gallaghe T.2020 SARS Coronavirus Redux . *Trends in Immunology* (Published online March 12, 2020 (doi:10.1016/j.it.2020.02.007).

4. Walls AC, Park YJ, Tortorici MA, Wall A, McGuire AT, Veesler D.2020 Structure, function, and antigenicity of the SARS-CoV-2 spike glycoprotein. *Cell* 180, 1-12 (doi: 10.1016/j.cell.2020.02.058).

5.Wrapp D, Wang N, Corbett KS, Goldsmith JA, Hsieh CL, Abiona O, Graham BS, McLellan JS. 2020 Cryo-EM structure of the 2019-nCoV-1spike in the prefusion conformation. *Science* 367: 1260-1263. (doi: 10.1126/science.abb2507)

6. Kirchdoerfer RN, Wang N, Pallesen J, Wrapp D, Turner HL, Cottrell CA, Corbett KS, Graham BS, McLellan JS, Ward AB.2018 Stabilized coronavirus spikes are resistant to conformational changes induced by receptor recognition or proteolysis.*Sci Rep* **8**: 15701-15701 (doi: 10.1038/s41598-018-34171-7).

7. Li F, Li W, Farzan M, Harrison SC. 2005 Structure of SARS coronavirus spike receptor-binding domain complexed with receptor. *Science* 309**:** 1864-1868. (doi: 10.1126/science.1116480).

8. Yan R, Zhang Y, Li Y, Xia L, Guo Y, Zhou Q.2020 Structural basis for the recognition of the SARS-CoV-2 by full-length human ACE2. *Science* 367, 1444-1448 (doi: 10.1126/science.abb2762)

9. Li F.2016 Structure, function, and evolution of coronavirus spike proteins.Annu. Rev.Virol. 3, 237-261. (doi: 10.1146/annurev-virology-110615-042301).

10. Farrell D.W., Speranskiy K., and Thorpe M.F. 2010 Generating stereochemically acceptable protein pathways. *Proteins* 78, 2908–2921.

11. Hu Y, Buehler MJ.2021 Comparative Analysis of Nanomechanical Features of Coronavirus Spike Proteins and Correlation with Lethality and Infection Rate. *Matter* 4, 265-275. (doi: 10.1016/j.matt.2020.10.032).

12. Chan K.H., Peiris J.S., Lam S.Y., Poon L.L., Yuen K.Y., and Seto W.H.2011 The effects of temperature and relative humidity on the viability of the sars coronavirus. *Adv Virol.* 734690 (doi: 10.1155/2011/734690).

13. Kumar S., Paul A., Chatterjee S., Pu¨tz S., Nehra N., Wang D.S., Nisar A., M Jennings C., and Parekh S.H. 2021 Effect of ambient temperature on respiratory tract cells exposed to sars-cov-2 viral mimicking nanospheres-an experimental study. *Biointerphases* 16, 011006.

14. Shang J., Ye G., Shi K., Wan Y., Luo C., Aihara H., Geng Q., Auerbach A., and Li F.2020 Structural basis of receptor recognition by sars-cov-2. Nature 581, 221–224.

15.Xue L, Rodrigues J, Kastritis P, Bonvin AMJJ, Vangone A.2016 PRODIGY: a web-server for predicting the binding affinity in protein-protein complexes. *Bioinformatics* 32, 3676-3678 (doi:10.1093/bioinformatics/btw514).

16. Jacobs DJ, Rader AJ, Kuhn LA, Thorpe MF. 2001 Protein flexibility predictions using graph theory. *Proteins*, 44, 150-165 (doi: 10.1002/prot.1081).

17. Ali A, Vijayan R.2020. Dynamics of the ACE2–SARS-CoV-2/SARS-CoV-1spike protein interface reveal unique mechanisms. *Sci Rep* **10,** 14214.

18. Malik A, Prahlad D, Kulkarni N, Kayal A.2020.Interfacial Water Molecules Make RBD of SPIKE Protein and Human ACE2 to Stick Together, bioRxiv 2020.06.15.152892.

19. Belouzard S, Millet JK, Licitra BN, Whittaker GR. 2012 Mechanisms of Coronavirus Cell Entry Mediated by the Viral Spike Protein. Viruses 4, 1011-1033. (doi: 10.3390/v4061011)

20. Ou X, Liu Y, Lei X. *et al.*2020 Characterization of spike glycoprotein of SARS-CoV-2 on virus entry and its immune cross-reactivity with SARS-CoV. *Nat Commun* **11,** 1620 (doi:10.1038/s41467-020-15562-9)

21. Shang W, Yang Y, Rao Y *et al.*2020 The outbreak of SARS-CoV-2 pneumonia calls for viral vaccines. *npj Vaccines* 5, 18 (2020).(doi: 10.1038/s41541-020-0170-0)

22. Liu C, Zhou Q, Li Y, Linda V. Garner LV, Watkins SP, Carter LJ, Smoot J, Gregg AC, Daniels AD, Jervey S, Albaiu D. 2020 Research and Development on Therapeutic Agents and Vaccines for COVID-19 and Related Human Coronavirus Diseases. *ACS Central Science* 6, 315-331 (doi: 10.1021/acscentsci.0c00272)

23. Atilgan AR, Durell SR, Jernigan RL, Demirel MC, Keskin O, Bahar I. 2001 Anisotropy of fluctuation dynamics of proteins with an elastic network model. *Biophys J* 80, 505-515 (doi: 10.1016/S0006-3495(01)76033-X).

24. Du Q, Beglov D, Roux B.2000. Solvation Free Energy of Polar and Nonpolar Molecules in Water: An Extended Interaction Site Integral Equation Theory in Three Dimensions, *The Journal of Physical Chemistry B* 104*:* 796-805 (doi: 10.1021/jp992712).

25. Kovalenko A, Hirata F.1998.Three-dimensional density profiles of water in contact with a solute of arbitrary shape: a RISM approach. *Chem. Phys. Lett.* 290: 237–244.

26. Fedotova MV, Kruchinin SE.2012. 1D-RISM study of glycine zwitterion hydration and ion-molecular complex formation in aqueous NaCl solutions. *J. Mol. Liq.* 169: 1–7 (doi: 10.1016/j.molliq.2012.03.008).

27. Chuev GN, Valiev M, M.V. Fedotova MV.2012. Integral equation theory of molecular solvation coupled with quantum mechanical/molecular mechanics method in NWChem package. *J. Chem. Theory Comput.* 8: 1246–1254 (doi:10.1021/ct2009297).

28. Fedotova MV, Kruchinin SE.2013. Hydration of para-aminobenzoic acid (PABA) and its anion—the view from statistical mechanics. *J. Mol. Liq.* 186: 90–97. (doi: 10.1016/j.molliq.2013.05.028).

29. Fedotova MV, Kruchinin SE.2013. The hydration of aniline and benzoic acid: analysis of radial and spatial distribution functions. *J. Mol. Liq.* 179: 27–33. (doi: 10.1016/j.molliq.2012.11.031).

30. Fedotova MV, Dmitrieva OA.2015. Ion-selective interactions of biologically relevant in organic ions with alanine zwitterion: a 3D-RISM study. *Amino Acids* 47: 1015–1023 (doi: 10.1007/s00726-015-1930-4).

31. Eiberweiser A, Nazet A, Kruchinin SE, Fedotova MV, Buchner R.2015. Hydration and ion binding of the osmolyte ectoine. *J. Phys. Chem. B* 119:15203–15211 (doi: 10.1021/acs.jpcb.5b09276).

32. Fedotova MV, Dmitrieva OA.2016. Proline hydration at low temperatures: its role in the protection of cell from freeze-induced stress. *Amino Acids* 48: 1685–1694. (doi: 10.1007/s00726-016-2232-1).

33. Fedotova MV, Kruchinin SE, Chuev GN.2017. Local ion hydration structure in aqueous

imidazolium-based ionic liquids: the effects of concentration and anion nature. *J. Mol. Liq.* 247: 100–108. (doi:10.1016/j.molliq.2017.09.087).

34. Dmitrieva OA, Fedotova MV, Buchner R.2017. Evidence for cooperative Na+ and Cl−binding by strongly hydrated l-proline. *Phys. Chem. Chem. Phys.* 19: 20474–20483. (doi:10.1039/c7cp04335j).

35. Shaukat S, Fedotova MV, Kruchinin SE, Bešter-Rogač M, Podlipnik C, Buchner R.2019. Hydration and ion association of aqueous choline chloride and chlorocholine chloride. *Phys. Chem. Chem. Phys.* 21:10970–10980 (doi:10.1039/c9cp01016e).

36. Fedotova MV. 2019.Compatible osmolytes - bioprotectants: is there a common link between their hydration and their protective action under abiotic stresses? *J. Mol. Liq.* 292: 111339. (doi: 10.1016/j.molliq.2019.111339).

37. Lue L, Blankschtein D.1992. Liquid-state theory of hydrocarbon-water systems: application to methane, ethane, and propane. *J. Phys. Chem.* 92: 8582–8594. (doi: 10.1021/j100200a069).

38. Wang J, Wolf RM, Caldwell JW, Kollman PA, Case DA.2004. Development and testing of a general amber force field. *J. Comput. Chem.* 25: 1157–1174. (doi: 10.1002/jcc.20035).

39. Case DA, Babin V, Berryman JT, Betz RM, Cai Q, Cerutti DS, Cheatham III TE, Darden TA, Duke RE, Gohlke et al. 2014. AMBER 14, University of California, San Francisco.

Supplementary Tables and Figures

Table S1: Interface residual interactions between CoV-1S glycoprotein receptor-binding domain (RBD) and human ACE2

SARS-CoV-RBD-hACE2 Complex

	Human Receptor	Virus RBD Domain	Affinity (PRODIGY)
1	TYR83	ASN473	The binding affinity (ΔG) is ΔG = **-11.1** (kcal mol^{-1}) The dissociation constant (K_d) at 25.0 ℃ is: K_d = **7.3E-09** (M) = 7.3 nM
2	GLN24	ASN473	
3	ASP38	TYR436	
4	GLU37	TYR491	
5	LYS353	TYR481	
6	LYS353	GLY482	
7	LYS353	GLY488	
8	TYR41	THR486	
9	GLU329	ARG426	

SARS-CoV-2-RBD-hACE2 Complex

	Human Receptor	Virus RBD Domain	Affinity (PRODIGY)
1	LYS353	GLY502	The binding affinity (ΔG) is ΔG = **-10.8** (kcal mol^{-1}) The dissociation constant (K_d) at 25.0 ℃ is: K_d = **1.2E-08** (M) = 12 nM
2	TYR41	THR500	
3	TYR41	ASN501	
4	ASP38	TYR449	
5	GLU35	GLN493	
6	THR27	TYR489	

Table S2: Interface interaction summary between Receptor-binding domain (RBD) of CoV-1and human ACE2

The complex SARS-CoV-RBD-hACE2
[+] No. of intermolecular contacts: 55
[+] No. of charged-charged contacts: 1
[+] No. of charged-polar contacts: 8
[+] No. of charged-apolar contacts: 19
[+] No. of polar-polar contacts: 2
[+] No. of apolar-polar contacts: 17
[+] No. of apolar-apolar contacts: 8
[+] Percentage of apolar NIS residues: 34.96
[+] Percentage of charged NIS residues: 27.36
[++] Predicted binding affinity (kcal.mol-1): -11.1
[++] Predicted dissociation constant (M) at 25.0˚C: 7.3e-09

The complex SARS-CoV2-RBD-hACE2
[+] No. of intermolecular contacts: 59
[+] No. of charged-charged contacts: 1
[+] No. of charged-polar contacts: 9
[+] No. of charged-apolar contacts: 18
[+] No. of polar-polar contacts: 4
[+] No. of apolar-polar contacts: 18
[+] No. of apolar-apolar contacts: 9
[+] Percentage of apolar NIS residues: 36.60
[+] Percentage of charged NIS residues: 25.43
[++] Predicted binding affinity (kcal.mol-1): -10.8
[++] Predicted dissociation constant (M) at 25.0˚C: 1.2e-08

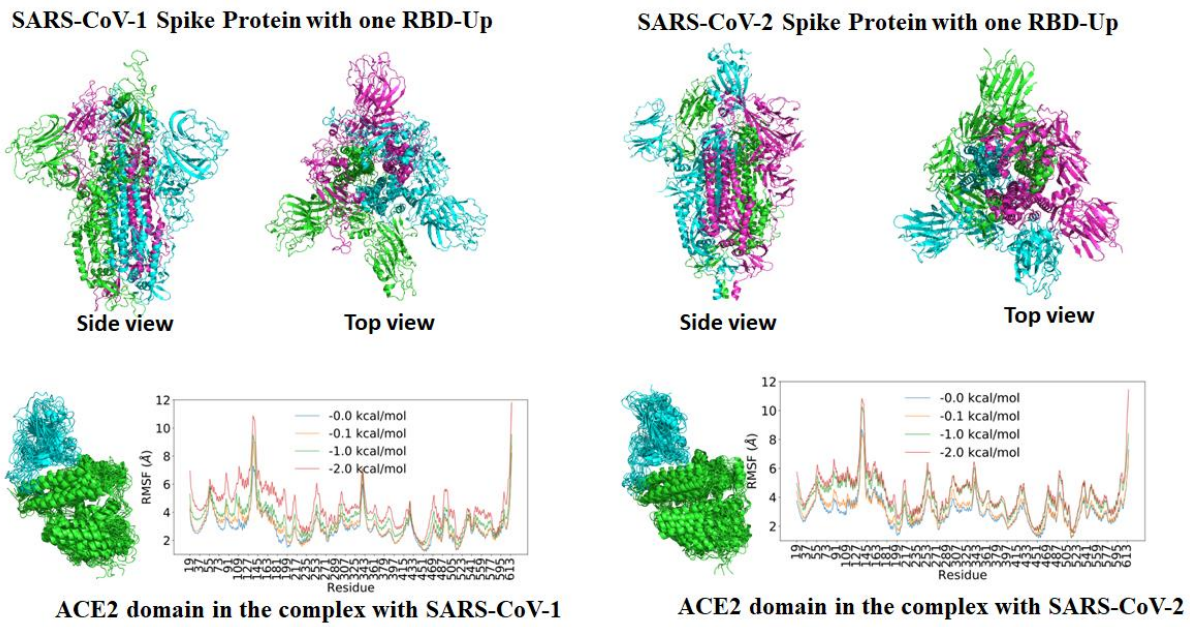

Fig.S1: Side and top view of SARS-CoV-1 and SARS-CoV-2 spike proteins, with RMSF of ACE2 bound with RBD-UP of the spikes.

Table S3: Average RMSF values of overall all the domains and RBD in the up state for SARS-CoV-1 and SARS-CoV-2 spike protein.

	All domains		RBD-Up	
Cut-off	SARS-CoV-1	SARS-CoV-2	SARS-CoV-1	SARS-CoV-2
-0.0kcal/mol	4.2±2.2Å	5.1±4.3Å	7.8±2.8Å	17.8±8.0Å
-0.1kcal/mol	4.9±2.8Å	6.1±5.0Å	11.9±4.1Å	19.5±8.8Å
-1.0kcal/mol	8.3±6.0Å	5.9±4.7Å	25.1±9.0Å	18.0±7.9Å
-2.0kcal/mol	9.2±6.6Å	6.1±4.3Å	27.9±9.9Å	16.4±6.8Å

Table S4: Average RMSF values of the ACE2 and the RBD of SARS-CoV-1 and SARS-CoV-2 in the complex.

	ACE2		RBD	
Cut-off	SARS-CoV-1	SARS-CoV-2	SARS-CoV-1	SARS-CoV-2
-0.0kcal/mol	2.9±1.0Å	3.0±1.0Å	4.3±1.9Å	4.0±1.7Å
-0.1kcal/mol	3.0±1.0Å	3.2±1.0Å	4.7±1.9Å	4.4±1.8Å
-1.0kcal/mol	3.5±1.1Å	4.0±1.3Å	5.7±2.1Å	4.8±1.9Å
-2.0kcal/mol	4.4±1.4Å	4.3±1.4Å	7.0±2.9Å	5.5±2.3Å

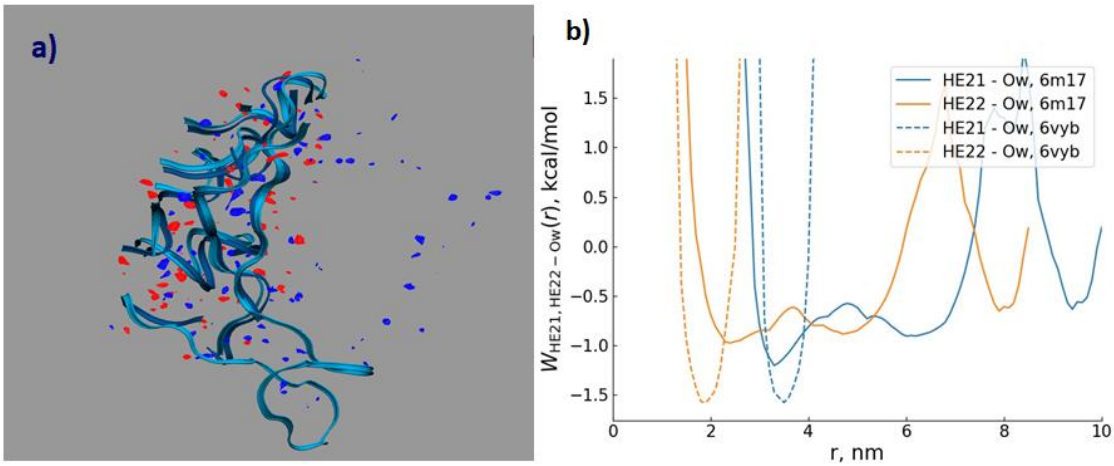

Fig.S2. Water distribution around RBD of SARS-CoV-2. (a) Differences in distributions of water oxygen (blue) and water hydrogens (red) between the CoV-2/hACE2 and CoV-2; (b) the pmf RBD-O and RBD-H for the CoV-2 and CoV-2/hACE2 complex. The RBD is indicated by blue ribbons, the RBD of CoV-2 is shown as background for the differences.